Continuum equations for dielectric response to macro-molecular assemblies at the nano scale

2004 J. Phys. A: Math. Gen. 37 9791

(http://iopscience.iop.org/0305-4470/37/41/012)

INSTITUTE OF PHYSICS PUBLISHING JOURNAL OF PHYSICS A: MATHEMATICAL AND GENERAL

J. Phys. A: Math. Gen. **37** (2004) 9791–9803 PII: S0305-4470(04)80600-0

Continuum equations for dielectric response to macro-molecular assemblies at the nano scale

Ridgway Scott[1], **Mercedes Boland**[2], **Kristina Rogale**[3] **and Ariel Fernández**[4,5]

[1] The Institute for Biophysical Dynamics, the Computation Institute, and the Departments of Computer Science and Mathematics, The University of Chicago, Chicago IL 60637, USA
[2] 100 Morningside Drive, #6B, New York, NY 10027, USA
[3] Program in Applied and Computation Mathematics, Princeton University, Princeton NJ 08544, USA
[4] Indiana University School of Informatics and Center for Computational Biology and Bioinformatics and Department of Biochemistry and Molecular Biology, Indiana University School of Medicine, 714 N Senate Ave, Indianapolis, IN 46250, USA
[5] Department of Computer Science, University of Chicago, Chicago, IL 60637, USA

Received 12 May 2004, in final form 22 July 2004
Published 29 September 2004
Online at stacks.iop.org/JPhysA/37/9791
doi:10.1088/0305-4470/37/41/012

Abstract

We study a frequency-dependent continuum model equation for electrostatics at the nano scale. It is motivated by the need to incorporate accurately the influence of dielectric correlations which are of the same length scale as the electrostatic fluctuations in protein–water systems. The model is based on a single parameter, a length scale for changes in the dielectric response, that is physically relevant. This parameter reflects the changes in the dielectric medium caused by local structuring of the molecules. We present three independent quantitative assessments of the model, including one in which the dielectric field is changing in time. The assessments involve modeling the local structuring of dielectrics around individual ions, explaining solvation of carbon nano-tube interiors and predicting accurately the electrostatic energy of ions in a carbon nano-tube. The latter involves comparing the frequency-dependent model equation directly with molecular dynamics simulations with explicit solvent. The model equation cannot be written as a differential equation but rather takes the form of a more general Fourier integral operator. It involves a non-local relationship between the polarization field and the electric field.

PACS numbers: 87.15.Aa, 41.20.Cv, 83.10.−y

(Some figures in this article are in colour only in the electronic version)

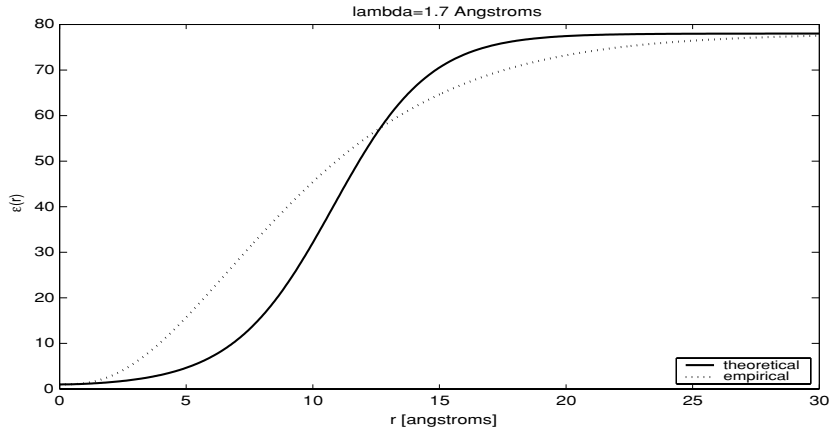

Figure 1. Comparison of empirical permittivity formula in [4] (dotted line) with the model (18) (solid line) where κ is defined in (4) with $\lambda = 1.7$. Plotted are the ratios of the effective permittivity experienced by a dipole to the vacuum permittivity as a function of the separation distance in Å, where the bulk permittivity is that of water.

Introduction

A frequently used, *ad hoc* model to describe the electrostatics at protein–water interfaces [1] assumes that the permittivity $\tilde{\epsilon}$ may be treated as a mean-field parameter that jumps from one value in the solvent to another in the protein. In that model, the electrostatic field satisfies the equation

$$\nabla \cdot (\tilde{\epsilon}(\mathbf{r})\nabla\phi(\mathbf{r})) = \rho(\mathbf{r}). \tag{1}$$

This model can be augmented by allowing the permittivity to vary smoothly [2–4] using *ad hoc* parameters to represent the transition, as is shown in figure 1. However, this ansatz does not reflect adequately the organization of water around a protein. In particular, it fails to capture the dielectric correlations which change significantly on this scale. The electric field around a protein can vary dramatically [5], so approximating the wave-number-dependent dielectric by a single value would not be expected to be very accurate, at least near a protein surface.

It might be hoped that (1) would provide a reasonable mean-field approximation, but we were surprised to find that it did not accurately predict the time-dependent electrostatic energy of solvated ions in a carbon nano-tube which we determined independently by doing all-atom molecular dynamics simulations with explicit solvent. We indicate in figure 2 the size of discrepancy that a model of the type (1) can have in practice.

Fortunately, we found that another model [6, 7] which explicitly accounts for the dielectric correlations does accurately predict the electrostatic energy of ions in a carbon nano-tube determined from our molecular dynamics simulations (see figure 3). That model represents the differential dielectric response as a function of wave number, as indicated in (4), whereas (1) only accounts for this variation via a mean-field approach.

Models for electrostatics of the type (1) have been utilized to simulate the screening effect of dielectrics near an ion [4]. However, such models require again an ad hoc representation of the permittivity as a function of the distance from some object. The concept of a dielectric is self-referential. That is, the polarization field determining the dielectric depends on the electric field alone, although the relationship may vary as the material constituency of the dielectric medium changes. Thus it would be of interest to have a model of electrostatics

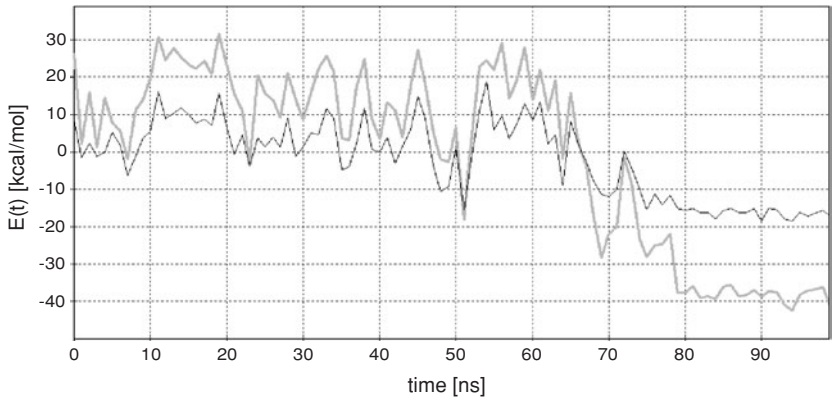

Figure 2. Electrostatic energy restricted only to the ions within nano-tube I (see section 4) in all configurations generated in the simulation. The explicit-solvent computation (grey line) is contrasted against the analytic computation (black line) computed with the model (1) with $\tilde{\epsilon}(r) = \epsilon_{\text{opt}} f(r)$ where $f(r)$ is the empirical expression [4] depicted in figure 1. The parameter ϵ_{opt} was chosen to balance the positive and negative errors in the figure and had a value of $\epsilon_{\text{opt}} = 11$.

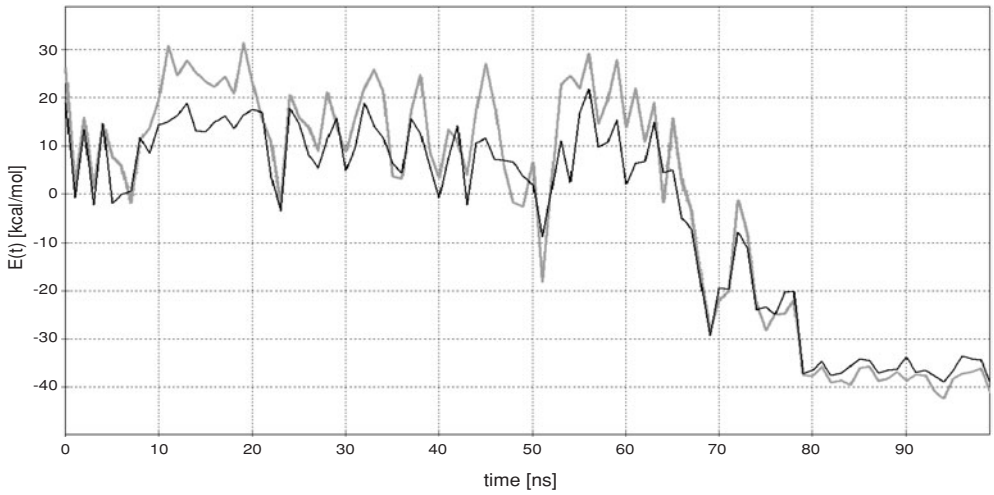

Figure 3. Over-all electrostatic energy restricted only to the ions within nano-tube I (see section 4) in all configurations generated in the simulation. The explicit-solvent computation (grey line) is contrasted against the analytic computation (black line) with average dielectric relaxation length $\langle\lambda\rangle_I = 3.26\lambda_b$.

which is intrinsic, as we consider here. Moreover, we will see that the form of the equation is fundamentally different from what would be obtained with a spatially varying dielectric of the form considered to date.

The model equation we utilize takes the form of a Fourier integral operator [8]. We present independent evaluations of the model. In one case, we consider the effect of ionic screening, and in two others we consider the behaviour of water and ions in a nano-tube. With only one free parameter, a length scale encoding the scale of dielectric response, we get excellent agreement over a broad range of physical/chemical systems.

1. Dielectric model

The fundamental equations of electrostatics for a collection of charges q_i at positions $\mathbf{r}_i$ can be derived from the simple expression

$$\nabla \cdot (\epsilon_0 \mathbf{e}) = \gamma(\mathbf{r}) := \sum_i q_i \delta(\mathbf{r} - \mathbf{r}_i) \tag{2}$$

where ϵ_0 is the permittivity of the vacuum. Here γ is the charge density (defined using the symbol ":=" in (2)) and $\mathbf{e}$ is the resulting electric field.

A dielectric medium is a collection of polar groups of atoms whose net charge is zero. In a dielectric medium we can write $\gamma = \rho - \nabla \cdot \mathbf{p}$ where $\mathbf{p}$ is the polarization field resulting from these charge groups, and thus we have $\nabla \cdot (\epsilon_0 \mathbf{e} + \mathbf{p}) = \rho$. Debye [9] observed that (on average) $\mathbf{p}$ is proportional to $\mathbf{e}$ where the constant of proportionality is an effective permittivity. However the relationship between $\mathbf{p}$ and $\mathbf{e}$ depends on frequency, ν. In particular, he found

$$\epsilon(\nu) = \epsilon_0 + \frac{\epsilon_1 - \epsilon_0}{1 + \tau_D^2 \nu^2} \tag{3}$$

where τ_D is the dielectric relaxation time, a property of the dielectric material, and ν is the temporal wave number. This dependence on temporal wave number has been verified experimentally (cf [10] for recent results and references to earlier work).

We are interested in electric fields which are *not* varying rapidly in time (i.e., $\nu \approx 0$) but rather spatially varying on the nanoscale. Thus we introduce the ansatz that the dielectric response depends on spatial wave number ξ proportional to a factor κ given by

$$\kappa(\xi) = \epsilon_0 + \frac{\epsilon_1 - \epsilon_0}{1 + |\lambda \xi|^2} \tag{4}$$

where λ is the characteristic *length* for dipole reorientation influence, another property of the dielectric material, and ξ is the spatial wave number. We will of course interpret the physical meaning of λ subsequently in this paper. The model (4) is similar to what is called the Lorentzian approximation and κ is called the *static* dielectric function [6]. In general, λ could be a matrix, allowing for anisotropy, but for the time being we will think of it as a scalar. We use empirical evidence to determine the length scale λ, which we find to be approximately 1.7 Å in bulk water [4].

The choice of ansatz (4) is based on several considerations. It is clear that the dielectric response should decrease to zero as the wave number is increased. Once the spatial wave lengths are comparable to, or smaller than, the size of a dielectric molecule, the ability of that molecule to respond to such frequencies will be reduced. In the limit, the fluctuations will be so rapid as to have no affect on a given molecule. Thus we conclude that we must have $\kappa(\xi) \to 0$ as $\xi \to \infty$, although this argument does not however suggest a particular analytical form.

The form (4) is consistent with the form suggested by Debye that can be derived from diffusion theory [9]. For any plane waves, the basic solutions of the Maxwell equations, we can change between time and space by relating the spatial wave number ξ to the temporal wave number ν by $c\xi = \nu$ where c is the speed of light. That is, if we drive the system at a frequency ν it will cause spatial fluctuations with wave number $\xi = \nu/c$. Thus it is reasonable to ask if the formulae (4) and (3) can be reconciled, where $\lambda = c\tau$. The typical values of τ_D are of the order of 10^{-10} seconds, with a higher frequency mode also identified [10]. However, the spatial dependence of permittivity (4) would introduce a time constant, $\lambda/c < 10^{-18}$ seconds, which is much smaller than what has been observed experimentally [10]. Moreover, this is several orders of magnitude smaller than the time scale of molecular

fluctuations of the water molecule. This suggests that the spatial dependence described here is an independent feature of the model, not simply a spatial manifestation of previously observed temporal–wave-number dependence of the permittivity.

Macromolecules induce changes in the electric field which have significant components for spatial wave numbers of the order of $10^{10}\,\mathrm{m}^{-1}$ and higher [5]. The response of dielectrics such as water to such spatial fluctuations in an electric field has been studied in the context of hydrated electrons for many years (see the references in [6]).

2. Basic equations

We can expand $\mathbf{e}$ and $\mathbf{p}$ in a Fourier series and use the Debye relationship (4) to relate the resulting coefficients in the series. That is, we have

$$\widehat{\mathbf{p}}(\xi) = (\kappa(\xi) - \epsilon_0)\,\widehat{\mathbf{e}}\,(\xi). \tag{5}$$

where here and subsequently we use the notation $\widehat{u}$ to denote the Fourier transform of a function u:

$$\widehat{u}(\xi) := \frac{1}{(2\pi)^{3/2}} \int_{\mathbb{R}^3} \mathrm{e}^{\mathrm{i}\xi\cdot\mathbf{r}} u(\mathbf{r})\,\mathrm{d}\mathbf{r}. \tag{6}$$

Therefore the basic equation is (using the inverse Fourier transform)

$$\nabla\cdot\left(\frac{1}{(2\pi)^{3/2}} \int_{\mathbb{R}^3} \mathrm{e}^{-\mathrm{i}\mathbf{r}\cdot\xi}\kappa(\xi)\,\widehat{\mathbf{e}}\,(\xi)\,\mathrm{d}\xi\right) = \rho(\mathbf{r}). \tag{7}$$

The equation (**5**) implies that the relationship between $\mathbf{p}$ and $\mathbf{e}$ is non-local [6, 7].

We can write $\mathbf{e} = \nabla\phi$ using Maxwell's equations. This provides the simple relation

$$\widehat{\phi}(\xi) = \frac{\widehat{\rho}(\xi)}{|\xi|^2\kappa(\xi)} \tag{8}$$

which can be used to compute ϕ (and thus $\mathbf{e}$) from ρ. Thus the electrostatic energy can be easily computed as

$$\int_{\mathbb{R}^3} \rho(\mathbf{r})\phi(\mathbf{r})\,\mathrm{d}\mathbf{r} = \int_{\mathbb{R}^3} \frac{|\widehat{\rho}(\xi)|^2}{|\xi|^2\kappa(\xi)}\,\mathrm{d}\xi. \tag{9}$$

The expression (7) can be simplified in certain limits. Thus, we have

$$\frac{1}{(2\pi)^{3/2}} \int_{\mathbb{R}^3} \mathrm{e}^{-\mathrm{i}\mathbf{r}\cdot\xi}\kappa(\xi)\,\widehat{\mathbf{e}}\,(\xi)\,\mathrm{d}\xi \approx \epsilon_j\mathbf{e}(\mathbf{r}) \tag{10}$$

where $j = 1$ when $\mathbf{e}$ is very smooth and $j = 0$ when $\mathbf{e}$ consists of only high frequencies. However, for general fields $\mathbf{e}$ it is not possible to approximate the Fourier integral in this way. The equation (7) involves a Fourier integral operator [8]. When λ does not vary as a function of the spatial variable $\mathbf{r}$, it is possible to write (7) as a fourth-order elliptic partial differential operator for the potential ϕ, due to the special form of $\kappa(\nu)$. To derive such an expression, we apply the operator $1 - \lambda^2\Delta$ to the equation (7). However, it is easier to calculate in Fourier space. Recall that the symbol (or Fourier transform) of this operator is $1 + \lambda^2|\xi|^2$, and observe that $(1 + \lambda^2|\xi|^2)\kappa(\xi) = \epsilon_1 + \epsilon_0\lambda^2|\xi|^2$. Multiplying (8) by $|\xi|^2\kappa(\xi)(1 + \lambda^2|\xi|^2)$ and comparing Fourier transforms, we find that

$$\nabla\cdot((\epsilon_1 + \epsilon_0\lambda^2\Delta)\nabla\phi) = \epsilon_1\Delta\phi + \epsilon_0\lambda^2\Delta^2\phi = (1 + \lambda^2\Delta)\rho \tag{11}$$

provided that λ is constant. However, if λ is a function that varies with $\mathbf{r}$ (see section 4) then (11) is no longer valid.

3. Ionic screening

The first question to ask with the model (7) is what the electric field (or potential) looks like for a single charge $\rho = \delta$. More precisely, (7) with $\rho = \delta$ defines a family of potentials $\phi = \phi_{\theta,\lambda}$ for any given θ and λ, where $\theta = \epsilon_0/\epsilon_1$. For water, we have $\theta = 0.013$. A change of variables implies that

$$\phi(\mathbf{r}) = \frac{1}{\epsilon_0 \lambda} \varphi_\theta(\mathbf{r}/\lambda) \tag{12}$$

where φ_θ is defined using the kernel

$$\kappa_\theta(\xi) = 1 + \frac{\theta^{-1} - 1}{1 + \xi^2}. \tag{13}$$

In the limit $\lambda \to \infty$ we find $\phi_{\theta,\infty} = \phi_0(r) = 1/4\pi\epsilon_0 r$ independent of θ.

The computation of φ_θ requires us to consider the Fourier transform of a radially symmetric function u (which is itself radially symmetric). The following formula holds:

$$|\xi|\widehat{u}(\xi) := \frac{4\pi}{(2\pi)^{3/2}} \int_0^\infty r u(r) \sin(|\xi| r)\, \mathrm{d}r \tag{14}$$

where $u(r)$ means $u(\mathbf{r})$ with $r = |\mathbf{r}|$. Thus we have

$$\varphi_\theta(\mathbf{r}) = \frac{1}{2\pi^2 r} \int_0^\infty \frac{\sin(r\rho)}{\rho \kappa_\theta(\rho)}\, \mathrm{d}\rho. \tag{15}$$

Thus we can determine that

$$\phi_{\theta,\lambda}(\mathbf{r}) = \phi_0(\mathbf{r})(\theta + (1-\theta)\, \mathrm{e}^{-r/\lambda\sqrt{1-\theta}}). \tag{16}$$

From this we can derive an empirical spatial permittivity dependence

$$\tilde{\epsilon}(r) := \frac{\|\nabla\phi_0(\mathbf{r})\|}{\|\nabla\phi_{\theta,\lambda}(\mathbf{r})\|} \tag{17}$$

$$= \epsilon_0 \left(\theta + (1-\theta)\left(1 + \frac{r}{\lambda\sqrt{1-\theta}}\right) \mathrm{e}^{-r/\lambda\sqrt{1-\theta}}\right)^{-1} \tag{18}$$

which we compare to the formula in [4] in figure 1 with $\lambda = 1.7$.

It is important to emphasize that (7) is not the same as (1), even though we have derived the expression for $\tilde{\epsilon}(\mathbf{r})$ from (7). The equation (7) provides an intrinsic representation of the relationship between the electric field and the polarization field. The expression $\tilde{\epsilon}(\mathbf{r})$ simply provides a spatial portrayal of this relationship in a particular case, but it is not an accurate representation for all frequencies (if indeed for any particular solution). Equation (7) can be applied in general contexts.

4. Spatial dependence of λ: nano-tube case study

As a second test, we now consider our model (7) as it would relate to the behaviour of a system of water in a carbon nano-tube. In this case, the parameter λ depends on the distance to elements that can cause structuring of the dielectric, such as hydrophobes would do with water. The value of λ represents a length scale below which fluctuations in external fields lead to a substantially reduced dielectric response. Recent experiments [11] have indicated that such effects might be expected to occur on very long scales, e.g., when two hydrophobic plates immersed in water are brought to within 0.1 micron of each other. We propose that allowing λ to vary spatially near elements that cause independent structuring of the dielectric

Table 1. The number of water molecules *per nanometre* length of nano-tube reported by various authors. The radii of the tubes are indicated by listing the number n of units for an (n:n) armchair configuration. The first author names indicate the following references: Hummer [19], Marti [20], Noon [22], Mashl [23]. The second column is the length of the nano-tubes in nanometres. It should be remembered that the results listed in the row marked 'this paper' involved a combination of water and ions in the tubes and thus cannot be directly compared.

First author	length (nm)	$n=5$	$n=6$	$n=7$	$n=8$	$n=9$	$n=10$	$n=12$	$n=16$
Hummer	1.34		3.73						
Noon	2.0			12	18	29			
Mashl	4.0	3.5	4	7.5	13.8	20.3	26	42.5	86.3
This paper	5.36			7.1		9.8			
Marti	7.45		1.88		7.52		16.9	30.1	

fluid provides a way to systematically model electrostatics of macro-molecular systems at the nanometre scale.

Carbon nano-tubes may provide insight into the functioning of ion channels [12, 13]. However, ion channels can introduce many factors that affect the electrical environment, including shape change, complex distribution of hydrophobes, polar groups and charged residues [14]. Thus carbon nano-tubes present a simpler, but non-trivial, environment in which to study the effects of confinement and structuring of dielectrics [15, 16, 7, 17]. However, this understanding can be applied to more complex situations as well.

Recently, there has been a significant interest in simulating the environment of carbon nano-tubes by molecular dynamics [18–23]. (The earlier work [15] was done in a smooth cylindrical tube with an *ad hoc* hydrophobic repulsive force at the wall.) There is a simple competition that determines the behaviour of water in a carbon nano-tube. On the one hand, the enclosing tube limits the fluctuations of the water molecules and thus reduces translational entropy. This causes the interior of the tubes to be drier than the surrounding bulk environment. For example, in [19] the typical number of water molecules in the tube is five, whereas a region of the same size in bulk would hold more than twenty molecules. But correspondingly, as the water environment becomes more structured due to the drying effect of the tube, the electrostatic contribution to hydrogen bonding gets enhanced as the screening effect of the dielectric diminishes. Table 1 collects results based on molecular dynamics simulations from many groups, indicating that longer and narrower tubes are drier. As we will show, water molecules in a carbon nano-tube form very strong hydrogen bonds that compensate energetically for the entropic energy loss.

Detailed predictions of the number of water molecules in a nano-tube would require a model recognizing the discrete nature of the possible packings of water molecules in a hydrophobic tube, as well as the discrete sizes of carbon nano-tubes available. However the competition between loss of entropy and gain in electrostatic energy can be estimated. For example, the entropic loss may be estimated as $\Delta S = k_B \log \Psi$ where k_B is Boltzmann's constant and Ψ is the quotient of the expected number of hydrogen-bond partners in the nano-tube over the expected number in bulk water.

Denote $\beta^{-1} = k_B T$, where T is absolute temperature. Then the rate of response in the dielectric is slowed down, due to the suppression of $\phi = (1 - \Psi)m$ hydrogen bond partners ($m = 4$ for bulk water) with neighbouring water molecules, by a factor

$$\mathrm{e}^{\beta(F_d d - T\Delta s)} = \mathrm{e}^{-(\phi^{-1}+1)\log\Psi} = \Psi^{-(1+1/\phi)} \tag{19}$$

where $F_d d = -k_B T \phi^{-1} \log \Psi$ is the potential energy barrier opposing the reorientation of a dipole d in a field F_d and $\Delta S = k_B \log \Psi$.

We assume a growth in correlation length commensurate with the slowing down of the reorientation of the dipoles. This is in analogy with the growth of a spatial order parameter at criticality. We estimate the change in λ as

$$\lambda = \lambda_b \Psi^{-(1+1/\phi)} \tag{20}$$

where $\lambda_b = 1.7$, the bulk value. The dependence of Ψ on $\mathbf{r}$ is taken [24] to be

$$\Psi(\mathbf{r}) = 1 - \mathrm{e}^{-\|\mathbf{r}-\mathbf{r}_t\|/\lambda_b} \tag{21}$$

where $\mathbf{r}_t$ denotes the closest point to $\mathbf{r}$ on the nano-tube wall. This form agrees closely with figure 2 in [23] (also see the data in figure 2 in [25]).

We can now identify the source of thermodynamic compensation for water confinement. The entropy decrease per mole due to confining a water molecule inside the nano-tube is $T\Delta S = Tk_B \log \Psi(r) = 0.601 \log \Psi(r)$ kcal/mole at $T = 303$K. The enthalpy increase due to concurrent losses in binding partnerships is $\Delta H = m(1 - \Psi(r))\epsilon_{HB} = 1.44(1 - \Psi(r))$ kcal/mole (for a reasonable in-bulk hydrogen-bond enthalpy decrease of $\epsilon_{HB} \approx 0.36$ kcal/mole [10]). Therefore $\Delta H - T\Delta S = 1.44(1 - \Psi(r)) - 0.601 \log \Psi(r)$ kcal/mole.

If it were not for the enhancement of the electrostatic energy due to the modified dielectric environment, it would be thermodynamically unfavourable for water to go into a nano-tube.

The enhancement of the electrostatic field for a hydrogen bond can be derived by considering the expression (18) using different values for λ (λ_b in the bulk and $\lambda(s)$ for a hydrogen bond at a distance s from the tube wall) and for r (the hydrogen bond lengths in the bulk and in the nano-tube). The substantial increase of λ as the distance to the wall is decreased leads to an enhancement of the electrostatic field for a hydrogen bond, even if the bond length is increased in the nano-tube over the typical length in bulk.

To assess the net result of the competition of these two effects, we carried out extensive molecular dynamics simulations, to be described in detail subsequently. We constructed *in silico* two carbon nano-tubes of 14 (I) and 18 (II) carbon-ring perimeter, that is, (7,7) and (9,9), respectively, 'arm-chair' form nano-tubes, each embedded in an ionic solution reservoir. These were uncapped single-wall nano-tubes of 20 hexagonal rings in length (≈53.6 Å), and the diameters are ≈9.45 Å (I) and ≈12.15 Å (II).

The expressions $\langle\Psi\rangle_I = 0.441$ and $\langle\Psi\rangle_{II} = 0.821$ are the average of (21) over the respective nano-tube interiors.

The electrostatic enhancement of a single water–water hydrogen bond in the nano-tube compensates for the free energy cost of confining the molecule in the nano-tube:

$$\begin{aligned} 5\epsilon_{HB} &\approx 2.5\,\text{kcal/mole} \\ &> \Delta H_I - T\Delta S_I = 1.61\,\text{kcal/mole} \\ 1.66\epsilon_{HB} &\approx 0.83\,\text{kcal/mole} \\ &> \Delta H_{II} - T\Delta S_{II} = 0.478\,\text{kcal/mole}. \end{aligned}$$

Thus a dramatic enhancement of electrostatic interactions inside nano-tubes results as their diameter is decreased, causing a qualitative change in the behaviour of the nano-tube as a modulator of ion-concentration gradients. This suggested that we measure this quantitatively using our model equation (7) and compare these predictions with the molecular dynamics simulations.

5. A dynamic simulation

Since the dielectric field depends on the electric field, it will vary dynamically if, say, ions are moving in the dielectric medium. Our model (7) automatically adjusts for such changes and accounts accurately for any frequency dependence (which would arise as ions move

differentially) as well. A system consisting of a carbon nano-tube immersed in a bath of ions and water provides such an opportunity to use the model in a dynamic environment. To simulate such a system, we used classical molecular dynamics, which we now describe in some detail.

In the molecular dynamics simulations, each nano-tube is regarded as a rotationally free rigid body, and the simulations were carried out for 100 ns at 303 K. We used explicit solvent with the TIP5P [26] water model. Two ion pairs K^+L^- and L^+Cl^- were chosen so that the counter-ions L^+ and L^- were sterically precluded from entering the nano-tube. The bulk L^+Cl^- to K^+L^- concentration ratio was fixed at 7:1 (other extreme ratios give similar results). The solution consisted of 11818 water molecules, 220 K^+L^- dissociated ion pairs and 1540 L^+Cl^- dissociated ion pairs.

The water model incorporates basis-set effects and has been shown to faithfully encompass the solvent polarizability [27]. Four molecular dynamics simulations for each nano-tube (I, II) as described in section 4 were performed adopting AMBER 7 force field covering 100 ns of real (physical) time. The initial conditions were chosen so that the nano-tubes were initially loaded with water molecules and allowed to equilibrate in a pure-water reservoir before being transferred to the ionic solution at $t = 0$. An 8 Å-cutoff has been imposed on the ranges of all electrostatic interactions. The numerical integration employs the Verlet algorithm [28] with a 5 fs step. A thermal bath coupling [29] was adopted to control the temperature at 303 K. Structures were saved every 10 ps. Carbon atoms are modelled as Lennard–Jones spheres with 3.4 Å cross-section and potential well depth 0.086 kcal/mol, as in sp2 carbons. The sp2 bond lengths, planar and torsional angles have harmonic distortion force constants fixed at 1002 kcal/(mol Å^2), 126 kcal/(mol rad^2) and 89 kcal/(mol rad^2), respectively. The carbon-water Lennard–Jones cross-section is 3.275 Å and the energy well is fixed at 0.1143 kcal/mol, a value which represents the polarization of the nano-tube wall via a quantum-mechanical configuration interaction, leading to a deeper Lennard–Jones well than would be the case without polarization effects.

Both K^+ and Cl^- penetrated the nano-tubes and eventually an equilibrium concentration was established. While the bulk ratio was preserved inside the wider nano-tube, in the narrow one, a steady 5:5 Cl^-/K^+ ratio was established after 80 ns, concurrently with a slight drying transition. This is commensurate with the predicted enhancement of the electrostatic fields which cannot sustain a charge imbalance inside the smaller nano-tube. The dependence of Cl^-/K^+ ratio on nano-tube diameter can be accounted for by determining differences in charge shielding, as can be quantified by comparing the parameters $\langle\Psi\rangle_I = 0.441$ and $\langle\Psi\rangle_{II} = 0.821$, cf equation (20).

The nano-tube interiors remain hydrated in spite of the entropic cost $T\Delta S$ associated with the confinement of water. Throughout the simulations there are 40 ± 2 and 51 ± 3 water molecules inside nano-tubes (I) and (II), respectively, except for a distinct drying transition at 80 ns in nano-tube (I).

A survey of results from the literature (see table 1) shows that these results are in reasonable agreement regarding the number of water molecules per unit length of the nano-tube. In particular, table 1 shows that the number of water molecules per unit length grows essentially quadratically as a function of the diameter, and it decreases with the length of the nano-tube. Our numbers do not compare directly since there are in addition ions in the channel, but they are provided for reference.

Our results indicate that hydration of the nano-tube takes place with a steady flux of 21 ± 2 water molecules/ns (I) and 24 ± 2 water molecules/ns (II). Due to the confinement, the average hydrogen-bond lifetime within the nano-tubes is 16 ps (I) and 4 ps (II) *versus* 1 ps in bulk water [30].

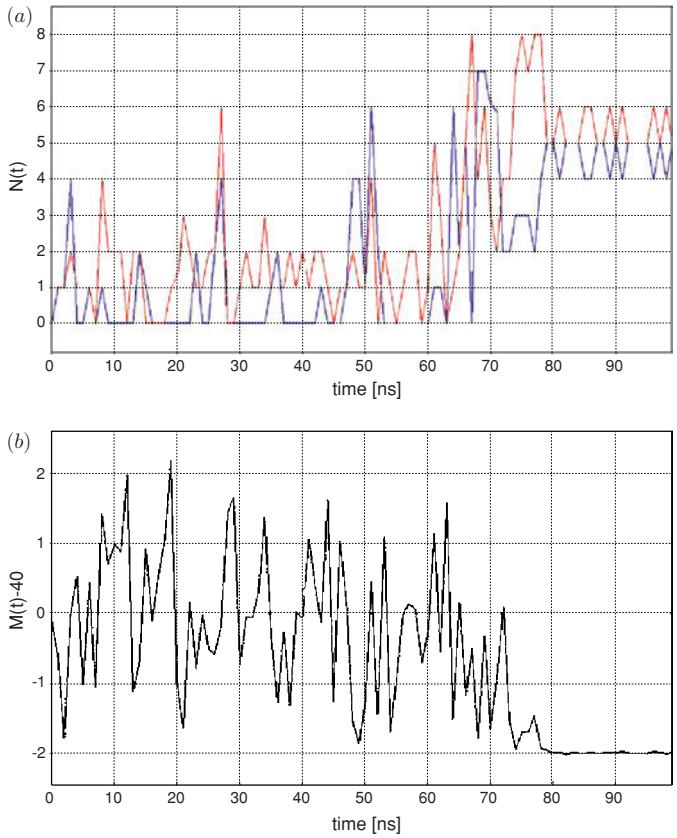

Figure 4. (*a*) Ion traffic in nano-tube I: the number $N(t)$ of Cl^- and K^+ ions inside the nano-tube at time t resolved at the ns time-scale over the 100 ns; this is a snapshot of the system at $t =$ 8 ns, and represents a short-lived configuration with a Cl^- / K^+ 4:1 ratio inside the nano-tube with 3 external bulky counter-ions (L^+) within 7 Å from the nano-tube. (*b*) Fluctuations around the average $\langle M \rangle = 40$ in the number of water molecules $M(t)$, at time t inside nano-tube I. The plotted values are averaged every 1ns. Notice the drying transition at about t* = 80 ns.

The dynamics of ion traffic in nano-tube I are displayed in figure 4(*a*), which shows the number $N(t)$ of Cl^- and K^+ ions inside the nano-tube at time t resolved at the ns time-scale over the 100 ns.

Figure 5(*a*) is a snapshot of the system at $t = 8$ ns, and represents a short-lived configuration with a Cl^- / K^+ 4:1 ratio inside the nano-tube with 3 external bulky counterions (L^+) within 7 Å from the nano-tube. Figure 5(*b*) is a snapshot of the system at $t = t^* = 80$ ns, when a dynamic steady state is reached with stoichiometric ratio 5:5 forming a chain of alternating Cl^- and K^+ ions. Once established at 80ns, this ratio *prevailed* for an additional 100 ns run with ± 1 fluctuations in the number of ions. Four simulations yielded a t^* dispersion within 10% of 80 ns. Similarly, a bulk 6:1 ratio yields $t^* \approx 44$ ns, a 5:1 ratio yields $t^* \approx 37$ ns and a 2:1 ratio yields $t^* \approx 19$ ns.

The steady 5:5 stoichiometry implies that a charge de-shielding due to severe water confinement makes it impossible to sustain a charge imbalance within nano-tube I, and that the proximity of bulky counterions from the outside is insufficient to counteract a charge imbalance (cf figure 4(*a*)). Furthermore, there is a slight 'drying transition' (Figure 4(*b*)) in

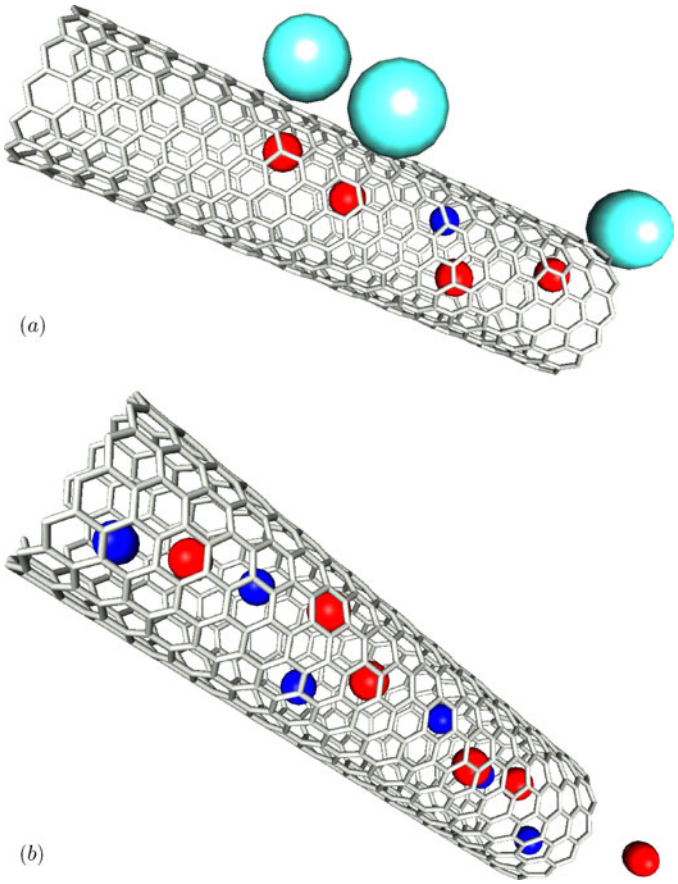

Figure 5. (*a*) Unstable ion configuration in nano-tube I with a Cl^-/K^+ 4:1 stoichiometry, occurring at $t = 8$ ns (cf figure 3). The charge imbalance inside the nano-tube is compensated externally by the presence of bulky L^+-counter-ions within 7 Å of the nano-tube wall. Cl^-, K^+ and L^+ are represented as red, blue and light blue balls of ionic radius 1.8, 1.38 and 6.1 Å, respectively. (*b*) Stable ion configuration at $t = t^* = 80$ ns inside nano-tube I with a steady 5:5 stoichiometry (cf figure 3).

nano-tube I concurrent with the charge balance (figure 3) reinforcing the charge de-shielding precisely for $t > t^* = 80$ ns.

By contrast, no appreciable variation from the bulk Cl^-/K^+ 7:1 ratio is observed inside the wider nano-tube II (figure 6): the 7:1 ratio is established at $t^* \approx 8$ ns and remains approximately steady for the remaining 92 ns. The charge imbalance inside the tube is compensated from the outside by the permanent presence of bulky counterions within 7 Å from the walls. The t^* dispersion was within 5% of this for four simulations.

The model equation (7) can be evaluated by computing the electrostatic interaction energy for all configurations of ions inside nano-tube I along the 100 ns simulation as shown in figure 3 (similarly satisfactory results are obtained for nano-tube II). To estimate the field $\mathbf{e}(\mathbf{r})$ at position $\mathbf{r}$ generated by the ion distribution in the nano-tube, we utilized the model equation (7) with an averaged λ as described following (20). Thus for our nano-tube I, we find $\langle\lambda\rangle_I = 3.26\lambda_b$ and for nano-tube II, we find $\langle\lambda\rangle_{II} = 1.6\lambda_b$. With these values of $\langle\lambda\rangle_I$ and $\langle\lambda\rangle_{II}$, we find that invariably the electrostatic energy predicted using (9) for ion concentrations in the nano-tubes agrees with data obtained from molecular dynamics experiments, averaged

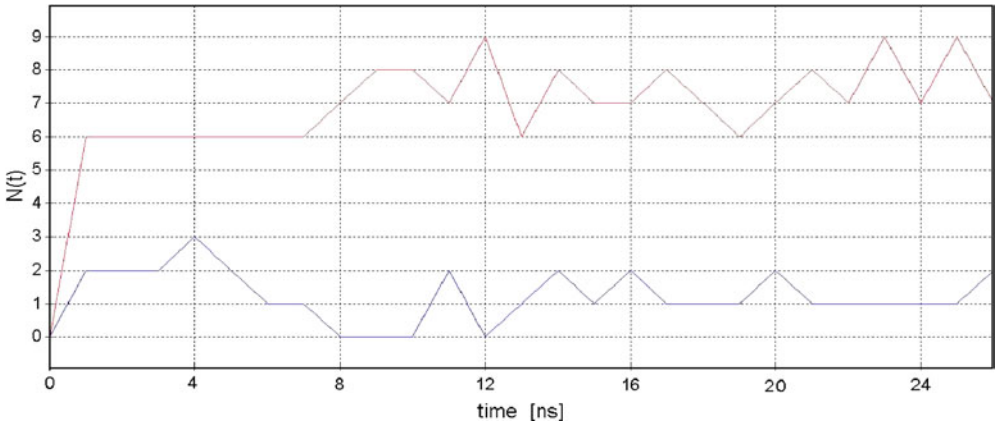

Figure 6. The traffic of Cl^- (red) and K^+ (blue) ions in nano-tube II represented as the number of ions, $N(t)$, of each type present inside the nano-tube at time t. The 100 ns simulation is examined at 1ns intervals. The steady-state regime actually extends in time until the end of the simulation, lasting at least 92 ns.

over 10 ns intervals, to within 5–15%, generated by the explicit-solvent all-atom simulation for all the ion configurations. The drying transition at $t = 80$ ns in nano-tube I provides a dynamic application of (7).

Finally, let us reconsider the model (1) with $\tilde{\epsilon}(r) = \epsilon_{\text{opt}} f(r)$ where $f(r)$ is the empirical expression [4] depicted in figure 1. The parameter ϵ_{opt} was chosen to balance the positive and negative errors in figure 2, and had a value of $\epsilon_{\text{opt}} = 11$. Thus it is clear that the model (1) cannot provide the same level of accuracy as (7).

6. Conclusions

A wave-number-dependent continuum model for electrostatics [6, 7] has been shown to predict nano-scale behaviour better than mean-field models. It was motivated by the need to incorporate accurately dielectric correlations. The model is based on a single parameter, a length scale that reflects the extent of local structuring of the dielectric molecules. We presented three independent quantitative uses of the model, including one in which the dielectric field is changing in time. The latter compares the wave-number-dependent model with molecular dynamics simulations with explicit solvent and demonstrates clearly the improvement over other models. The frequency-dependent model has also been used successfully [31, 32] to quantify the extent of wrapping of hydrogen bonds on the surface of proteins.

References

[1] Madura J D *et al* 1995 Electrostatics and diffusion of molecules in solution: simulations with the University of Houston Brownian Dynamics program *Comput. Phys. Commun.* **91** 57–95

[2] Ramsetin J and Lavery R 1988 Energetic coupling between DNA bending and base pair opening *Proc. Natl Acad. Sci. USA.* **85** 7231–5

[3] Cheng W, Wang C X, Chen W Z, Xu Y W and Shi Y Y 1998 Investigating the dielectric effects of channel pore water on the electrostatic barriers of the permeation ion by the finite difference Poisson–Boltzmann method *Eur. Biophys. J.* **27** 105–12

[4] Shen M-Y and Freed K F 2002 Long time dynamics of met-enkephalin: comparison of explicit and implicit solvent models *Biophys. J.* **82** 1791–808

[5] Suydam I T and Boxer S G 2003 Vibrational Stark effects calibrate the sensitivity of vibrational probes for electric fields in proteins *Biochemistry* **42** 12050–5
[6] Kornyshev A A and Nitzan A 2001 Effect of overscreeming on the localization of hydrated electrons *Z. Phys. Chem.* **215** 701–15
[7] Fernández A 2002 Intramolecular modulation of electric fields in folding proteins *Phys. Lett.* A **299** 217–20
[8] Duistermaat J J 1996 *Fourier Integral Operators* (Berlin: Springer)
[9] Debye P 1945 *Polar Molecules* (New York: Dover)
[10] Kaatze U, Behrends R and Pottel R 2002 Hydrogen network fluctuations and dielectric spectrometry of liquids *J. Non-Cryst. Solids* 305 19–28
[11] Lum K, Chandler D and Weeks J D 1999 Hydrophobicity at small and large length scales *J. Phys. Chem.* **103** 4570–7
[12] Berneche S and Roux B 2001 Energetics of ion conduction through the K+ channel *Nature* **414** 73–7
[13] Gullingsrud J, Kosztin D and Schulten K 2001 Structural determinants of MscL gating studied by molecular dynamics simulations *Biophys. J.* **80** 2074–81
[14] Tieleman D P, Biggin P, Smith G and Sansom M 2001 Simulation approaches ion channel structure–function relationships *Q. Rev. Biophys.* **34** 473–561
[15] Lynden-Bell R M and Rasaiah J C 1996 Mobility and solvation of ions in channels *J. Chem. Phys.* **105** 9266–80
[16] Zahab A, Spina L, Poncharal P and Marlière C 2000 Water-vapor effect on the electrical conductivity of a single-walled carbon nanotube *Phys. Rev.* B **62** 10000–3
[17] Fernández A and Scheraga H A 2003 Insufficiently dehydrated hydrogen bonds as determinants of protein interactions *Proc. Natl Acad. Sci. USA.* **100** 113–8
[18] Walther J H, Jaffe R, Halicioglu T and Koumoutsakos P 2000 Molecular dynamics simulations of carbon nanotubes in water *Proc. 2000 Summer Program (Stanford Center for Turbulence Research)*
[19] Hummer G, Rasaiah J C and Noworyta J P 2001 Water conduction through the hydrophobic channel of a carbon nanotube *Nature* **414** 188–90
[20] Martí J and Gordillo M C 2001 Temperature effects on the static and dynamic properties of liquid water inside nanotubes *Phys. Rev.* E **64** 021504
[21] Koga K, Gao G T, Tanaka H and Zeng X C 2001 Formation of ordered ice nanotubes inside carbon nanotubes *Nature* **412** 802–5
[22] Noon W H, Ausman K D, Smalley R E and Ma J 2002 Helical ice-sheets inside carbon nanotubes in the physiological condition *Chem. Phys. Lett.* **355** 445–8
[23] Mashl R J, Joseph S, Aluru N R and Jakobsson E 2003 Anomalously immobilized water: a new water phase induced by confinement in nanotubes *Nano Lett.* **3** 589–92
[24] McQuarrie D A 2000 *Statistical Mechanics* (MillValley, CA: University Science Books)
[25] Gordillo M C and Martí J 2000 Hydrogen bond structure of liquid water confined in nanotubes *Chem. Phys. Lett.* **329** 341–5
[26] Mahoney M W and Jorgensen W L 2000 A five-site model for liquid water and the reproduction of the density anomaly by rigid, nonpolarizable potential functions *J. Chem. Phys.* **112** 8910–22
[27] Stern H A, Rittner F, Berne B J and Friesner R A 2001 Combined fluctuating charge and polarizable dipole models: application to a five-site water potential function *J. Chem. Phys.* **115** 2237–51
[28] Allen M P and Tildesley D J 1989 *Computer Simulation of Liquids* (Oxford: Clarendon)
[29] Berendsen H J, Postma J P, van Gunsteren W F, Di Nola A and Haak J R 1984 Molecular dynamics with coupling to an external bath *J. Phys. Chem.* **81** 3684–90
[30] Berezhkovskii A and Hummer G 2002 Single-file transport of water molecules through a carbon nanotube *Phys. Rev. Lett.* **89** 064503
[31] Fernández A, Sosnick T R and Colubri A 2002 Dynamics of hydrogen bond desolvation in protein folding *J. Mol. Biol.* **321** 659–75
[32] Fernández A and Scott L R 2003 Dehydron: a structurally encoded signal for protein interaction *Biophys. J.* **85** 1914–28